



Dual internal functionalization of imogolite nanotubes as evidenced by optical properties of Nile red

Pierre Picot, Frédéric Gobeaux, Thibaud Coradin, Antoine Thill

► To cite this version:

Pierre Picot, Frédéric Gobeaux, Thibaud Coradin, Antoine Thill. Dual internal functionalization of imogolite nanotubes as evidenced by optical properties of Nile red. Applied Clay Science, 2019, 178, pp.105133. 10.1016/j.clay.2019.105133 . cea-02139490

HAL Id: cea-02139490

<https://cea.hal.science/cea-02139490>

Submitted on 24 May 2019

HAL is a multi-disciplinary open access archive for the deposit and dissemination of scientific research documents, whether they are published or not. The documents may come from teaching and research institutions in France or abroad, or from public or private research centers.

L'archive ouverte pluridisciplinaire **HAL**, est destinée au dépôt et à la diffusion de documents scientifiques de niveau recherche, publiés ou non, émanant des établissements d'enseignement et de recherche français ou étrangers, des laboratoires publics ou privés.

Abstract. Hybrid imogolites have been prepared by combining methyltrimethoxysilane with various organosilanes (Si-R) to obtain nanotubes with a bi-functional internal cavity. With an initial doping ratio Si-R/Si of 5%, nanotubes remain the major product in the samples and their diameter is not modified compared to pristine methyl imogolite (Imo-CH₃). The nanotube wall's internal polarity and reactivity is significantly changed as evidenced by using a solvatochromic dye (Nile red). This research opens many possibilities to bring selectivity to the internal cavity or to manipulate the properties of trapped organic molecules.

1. Introduction.

Imogolite (Imo) is a natural aluminosilicate nanotube (Yoshinaga and Aomine, 1962). Its chemical composition is (OH)₃Al₂O₃Si(OH) (Cradwick et al. 1972). The nanotubes are single-walled with a large curvature. The internal diameter of synthetic Imo is about 1 nm with a wall thickness of 0.6 nm. The curvature of the nanotube is partly due to the mismatch in distance between the relaxed size of the silicon tetrahedra (2.6 nm) and the O-O distances of the lacuna of a flat aluminum dioctahedric sheet (2.9 nm) where Si establishes three Si-O-Al bonds. This size mismatch alone is however not sufficient to explain the curvature. The intramolecular OH bonds between the internal silanol groups are also responsible for the stabilization of a zig-zag configuration of Imo and contribute to their very high curvature (Lee et al. 2011).

Since their discovery and their first synthesis more than forty years ago, many modifications of the wall composition as well as external and internal surfaces have been achieved (Arancibia-Miranda and Escudey 2016). In particular, the group of Bonelli unraveled a one-pot process to produce hybrid Imo nanotubes where the internal silanol groups are completely replaced by Si-CH₃ groups (Bottero et al. 2011). This synthesis produces nanotubes with a slightly larger internal diameter (*ca.* 1.8 nm), probably due to the absence of intramolecular hydrogen bonds. The hybrid Imo (Imo-CH₃) form stable dispersions but are always associated in small bundles (Boyer et al. 2014). Boyer et al. (2014) also showed that the inside of the hybrid nanotubes has an electronic density lower than water. Thus, the cavity of the Imo-CH₃ is hydrophobic and small enough to prevent water from wetting the internal pore surface (Liao et al., 2018). However, Imo-CH₃ are able to trap small organic molecules in their cavity (Amara et al. 2015; Picot et al. 2016).

35 In this paper, the possibility to incorporate an additional organic function within the internal cavity
36 of Imo-CH₃ nanotubes is established. This functionalization is obtained through the partial
37 replacement of the Si-CH₃ groups by other Si-R groups. We attempted to substitute 5% of the Si-CH₃
38 groups, which corresponds to one Si-R group per nanotube circumference. This ratio was however
39 difficult to detect and to quantify with standard analytical techniques. Nevertheless, the reactivity of
40 the internal cavity towards organic molecules is strongly modified by this additional
41 functionalization, as illustrated by using Nile red (NR), a solvatochromic hydrophobic dye.

42 2. Materials and Methods

43 Imo-CH₃ and functionalized Imo-CH₃ with a modified internal organic layer were prepared using a
44 protocol inspired by Bottero *et al.* (2011). Briefly, 80 mM aluminum-tri-sec butoxide (ASB) was
45 added to HCl_{aq} solution with a HCl/Al molar ratio of 0.5 and stirred during one hour. Then, silicon
46 precursors were added to obtain a Si/Al molar ratio of 0.575. Methyltrimethoxysilane is used as the
47 main silane. For the new surface function of the internal organic layer, trimethoxysilanes are used
48 bearing the following functional groups: 3-bromopropyl, chloromethyl, 3-aminopropyl, vinyl and 3-
49 mercaptopropyl. An initial ratio of 5%, defined as the molar ratio between Si-R silane and total
50 amount of Si, was used. For vinyl group, higher ratios (20 and 50%) were also tested. The dispersions
51 were kept in an oven for 5 days at 90°C and then dialyzed against MilliQ water using a 10 kDa
52 membrane until the conductivity of the external phase reaches 4 μS·cm⁻¹. In the following, the pristine
53 Imo-CH₃ is called methyl. The 5% doped Imo are called by the name of the end group of the
54 additional organosilane, i.e. bromo, chloro, amino, vinyl and mercapto.

55 Details on the characterization methods are given as supplementary information.

56

57 3. Results and Discussions

58 For all added silanes, nanotubes are obtained as the main product. The small angle X-ray scattering
59 (SAXS) signals obtained after dialysis for all the samples are reported in Figure 1a. The main feature
60 of the SAXS curves is the presence of clear oscillations due to a monodisperse diameter of the
61 nanotubes. The positions of the second and third intensity minimum of these oscillations, that are
62 very sensitive to the nanotube diameter, are similar for all nanotubes. However, the shape of the
63 curves changes. For vinyl- and mercapto-Imo, the slope of the low q range scattering signal is
64 modified and the position of the first intensity minimum is shifted to a larger q value. This shift may
65 be due to a modification of the internal electronic density or to the presence of a high proportion of
66 side products (allophane, proto-Imo or aluminum hydroxide platelets) (Picot *et al.* 2018). Methyl-,
67 chloro-, bromo- and amino-Imo display very similar SAXS curves. Cryo-TEM pictures of the bromo-,
68 amino- and mercapto-Imo (Figure 1b-d) clearly show the presence of side-products: Gibbsite platelets

(highlighted by black arrows in Figure 1c and 1d) and many proto-Imo and allophane. Cryo-TEM also suggests that the bromo-Imo (Figure 1b) contains much more proto-Imo and allophane than the amino-Imo, for example (Figure 1c).

The IR spectra of the synthesized hybrid Imos are reported in Figure 2. The dominant tubular nature of the products is clearly visible with the presence of a doublet in the 960–900 cm^{-1} range (Boyer et al. 2014; Amara et al. 2015; Picot et al. 2016). These bands are attributed to the Si–O stretching vibrations. In the Imo local structure, the three Si–O bonds are not all equivalent with respect to the nanotube axis. Therefore, two components at 910 and 955 cm^{-1} are observed depending on the angle between the tube axis and the Si–O bonds. This is not the case for allophane or proto-Imo for which a single band at 940 cm^{-1} is observed. The relative intensity of the two bands (910/955 cm^{-1}), linked to the proportion of side products and notably to the presence of proto-Imo and/or allophane (Picot et al. 2018), is changing from one hybrid to another depending on the introduced silane. On this basis, the hybrids with the most side products should be the chloro- and mercapto-Imo whereas the methyl-, amino- and vinyl-Imo should contain less of these. Moreover, for vinyl- and mercapto-Imo, the presence of aluminum hydroxide is evidenced by additional peaks at 1020 cm^{-1} and in the 3700–3400 cm^{-1} range. The characteristic peaks of methyl-Imo are also noticed at 782, 1275, 2918 and 2976 cm^{-1} for the Si–C stretching and methyl rocking, CH_3 symmetric deformation in Si– CH_3 and finally symmetric and asymmetric stretching of C–H in CH_3 , respectively (Bottero et al. 2011; Boyer et al. 2014; Liao et al. 2017). For all introduced groups, slight modifications of these later bands are visible (inset Figure 2).

In contrast, vibration bands signaling for the incorporation of added silanes are not clearly visible on the IR spectra, as could be expected for their low relative content (5% maximum only). Only the vinyl groups are visible with the typical =C–H stretching at 3080 and 3060 cm^{-1} (see inset of Figure 2). Moreover, two other contributions at 1615 and 1420 cm^{-1} associated to C=C stretching and to the bending in the plane of =C–H, respectively, are identifiable (inset (b) Figure S1) (Larkin 2011; Silverstein et al. 2015). The relative intensity of these four peaks increases with the initial amount of the vinyl-bearing silane, supporting their attribution.

As an alternative method to evidence the successful doping of the internal organic layer, it can be assumed that the presence of an additional chemical group could change the polarity of the cavity. Therefore, NR, a solvatochromic hydrophobic molecule, is used as a probe of the modification of the internal organic layer (Hess et al. 2013; Martin et al. 2016; Singappuli-Arachchige et al. 2016). The optical properties of NR are very sensitive to its environment, displaying a bathochromic shift of its absorption maximum of more than 100 nm when it is transferred from an apolar to a polar solvent (Dutta et al. 1996; Dias et al. 1999; Hazra et al. 2004; Jose and Burgess 2006). NR was transferred from a dodecane solution to an aqueous dispersion of the Imo- CH_3 through a liquid/liquid extraction

104 (Picot et al. 2016). It was noticed that no phase transfer of the dye occurred if pure water or an aqueous
105 dispersion of Imo (Imo-OH) were used (Figure S2). Imo-OH and Imo-CH₃ have almost the same
106 external surface covered with Al₂-(μOH) groups. The fact that no significant adsorption of NR is
107 observed on Imo-OH, even after prolonged contact time, disqualifies an external surface adsorption
108 on Imo-CH₃ and explains the very efficient liquid-liquid extraction of NR. Based on such experiment
109 and on the results obtained by Amara et al. (2015), the conclusion is that NR molecules are mainly
110 trapped in the internal cavity of Imo-CH₃ nanotubes.

111 The UV-vis spectra of the dispersions obtained after extraction of the dye by the different doped
112 hybrid Imo are significantly changed (Figure 3). In dodecane (an apolar solvent), NR exhibits a
113 yellow color with an absorption maximum at 491 nm. In polar ones like ethanol, it is red/pink with
114 the absorption maximum shifted to 549 nm. After NR extraction, the nanotube dispersions have a
115 strong coloration going from pink for amino-Imo to blue for mercapto-Imo. The measured
116 bathochromic shift of the dye absorption maximum within the nanotubes compared to the initial
117 dodecane solution is, in all cases, larger than the one observed with ethanol. For methyl-Imo, this
118 maximum is at 556 nm and it shifts up to 589.5 nm for the mercapto-Imo. Thus, upon interaction with
119 hybrid nanotubes, NR has clearly taken a color typical of a polar solvent. A change in the spectral
120 shape is also noticed for almost all samples compared to methyl-Imo, with up to three distinct
121 absorption bands being clearly identified. The main emission band of NR extracted from dodecane
122 by the different doped hybrid Imo also showed a significant shift of its maximum as a function of the
123 doping moiety (figure S3)

124 . Importantly, by measuring the dye concentration in the dodecane phase at the end of the extraction
125 process, it was possible to determine the concentration of the extracted NR inside the different
126 nanotubes. This concentration is 1.25 mg of dye per gram of Imo for all doped hybrid nanotubes.

127 Two effects can explain these observations. First, theoretical predictions of Elliott et al.(2017) using
128 DFT calculations suggested that the nanocavity of Imo has an intrinsic polarity that could be strongly
129 influenced by modifications of the internal surface. The present results would therefore constitute an
130 experimental confirmation of their calculation. Second, an effective 5% doping corresponds to one
131 organosilane group every 5.5 Å. The determined NR concentration within the nanotube (1.25 mg·g⁻¹)
132 corresponds to approximately one molecule every 360 Å along the Imo nanotube axis. Hence, the
133 doping organosilane dye ratio would be 65. Therefore, direct physical or chemical interactions
134 between NR and the doping organic moieties are highly plausible even at 5% doping. It should also
135 be noticed that the side products of the imogolite synthesis (allophane, proto-imogolite or gibbsite)
136 might also interact with the dye and contribute to its optical response, a point that will require further
137 studies.

138

139 4. Conclusion

140 Hybrid nanotubes with an internal Si-CH₃ surface doped with various Si-R chemical groups have
141 been obtained. The doping agent does not significantly modify the affinity of Nile red for the internal
142 cavity. However, the polarity of the nanotube wall is strongly modified by the presence of the doping
143 organosilanes, as evidenced by the strong variations of NR optical responses after entrapment. This
144 demonstrates that the proposed synthesis allows for the preparation of Imo nanotubes with a bi-
145 functionalized internal surface and opens many possibilities to improve the specificity of the cavity
146 towards targeted organic molecules and/or to tune the properties of encapsulated species, with
147 foreseeable applications in energy harvesting, remediation and sensing devices.

148 Acknowledgements.

149 This research is supported by public grant overseen by the French National Research Agency (ANR)
150 as part of the “Investissements d’Avenir” program (Labex NanoSaclay, reference: ANR-10-LABX-
151 0035). We thanks the Région Ile-de-France for PhD funding (HIPPOP grant) in the framework of
152 C’Nano IdF. C’Nano-IdF is the nanoscience competence center of Paris Region, supported by CNRS,
153 CEA, MESR and Région Ile-de-France. Cryo-TEM observations were made thanks to
154 “Investissements d’Avenir” LabEx PALM (ANR-10-LABX-0039-PALM). We thank Jéril
155 Degrouard for his time and his help. We warmly thank Faïza Bergaya for her time and advices which
156 improved this manuscript.

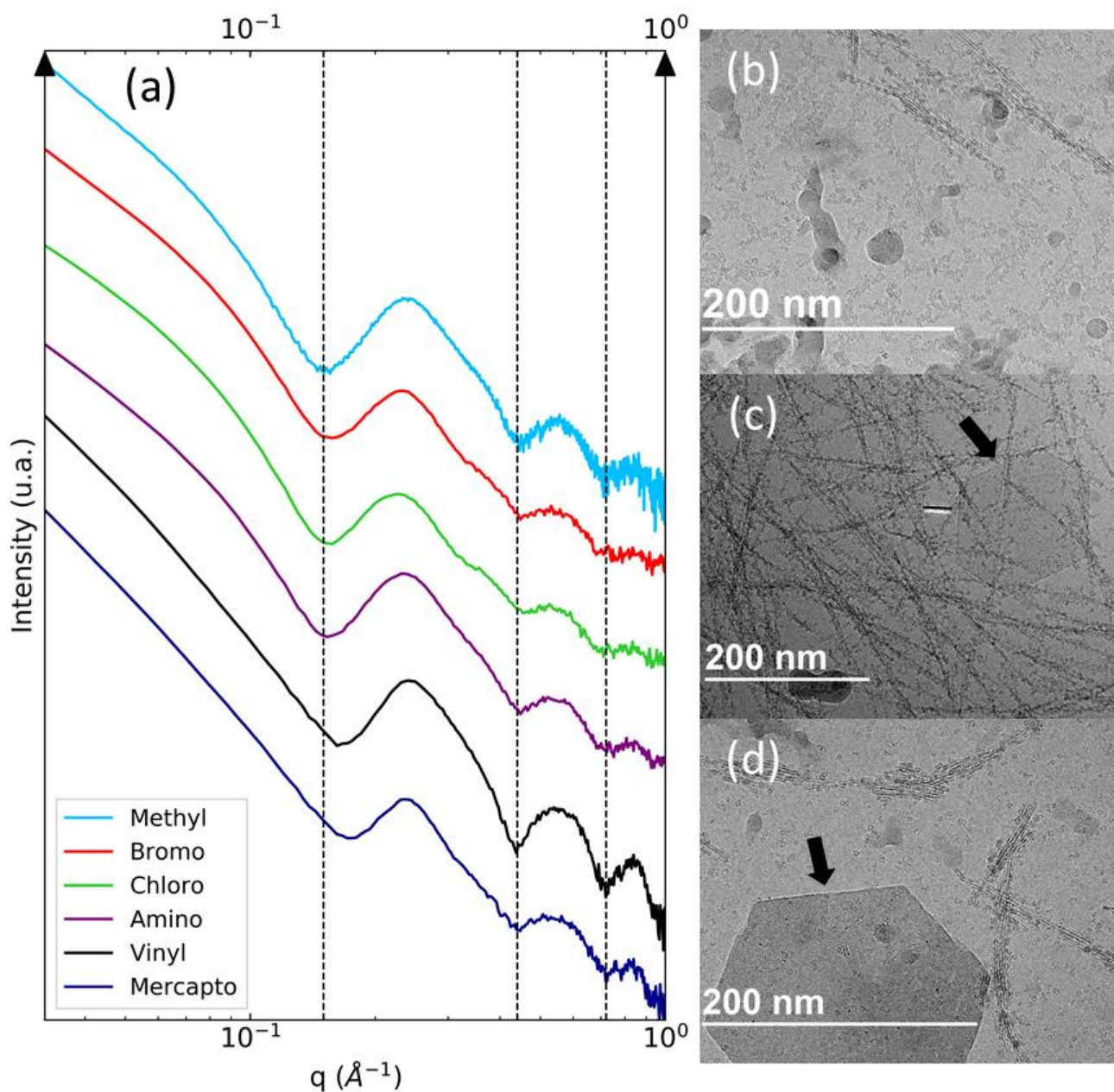
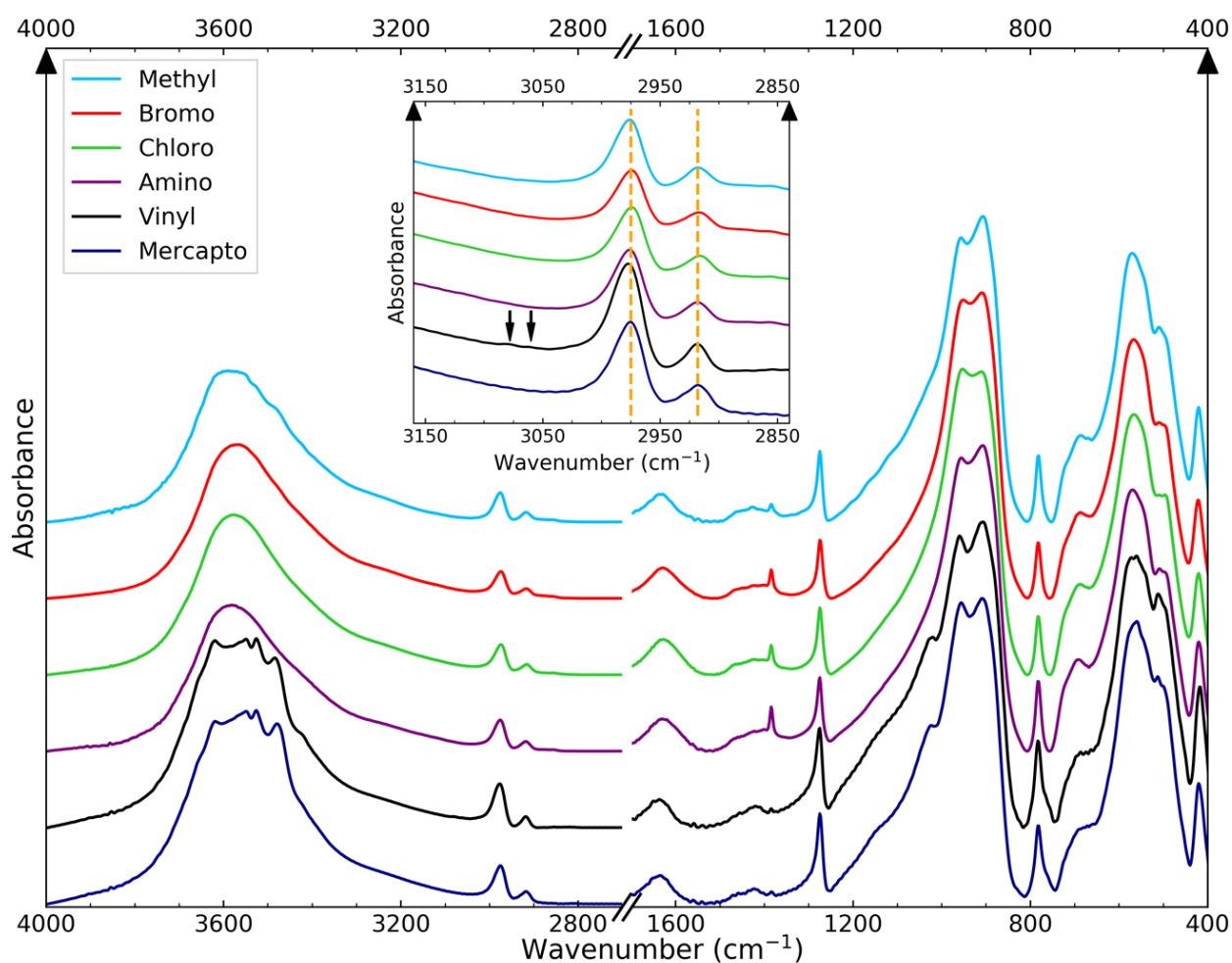


Figure 1 - SAXS curves (a) of methyl-Imo (cyan) and doped nanotubes: bromo (red), chloro (green), amino (purple), vinyl (black) and dark blue (mercapto). Dashed lines highlight the position of the first, second and third intensity minimum. Cryo-TEM images of bromo- (b), amino- (c) and mercapto-Imo (d). Black arrows highlight the presence of aluminum hydroxide platelets.



159

Figure 2 - IR spectra of methyl-Imo (cyan) and doped nanotubes: bromo (red), chloro (green), amino (purple), vinyl (black) and dark blue (mercapto). Inset is a zoom of the 3150 – 2850 cm^{-1} area. Orange dashed lines denote the position of antisymmetric and symmetric stretching of C–H in CH_3 . The two arrows highlight the peaks of vinyl groups associated to the $=\text{C–H}$ stretching.

160

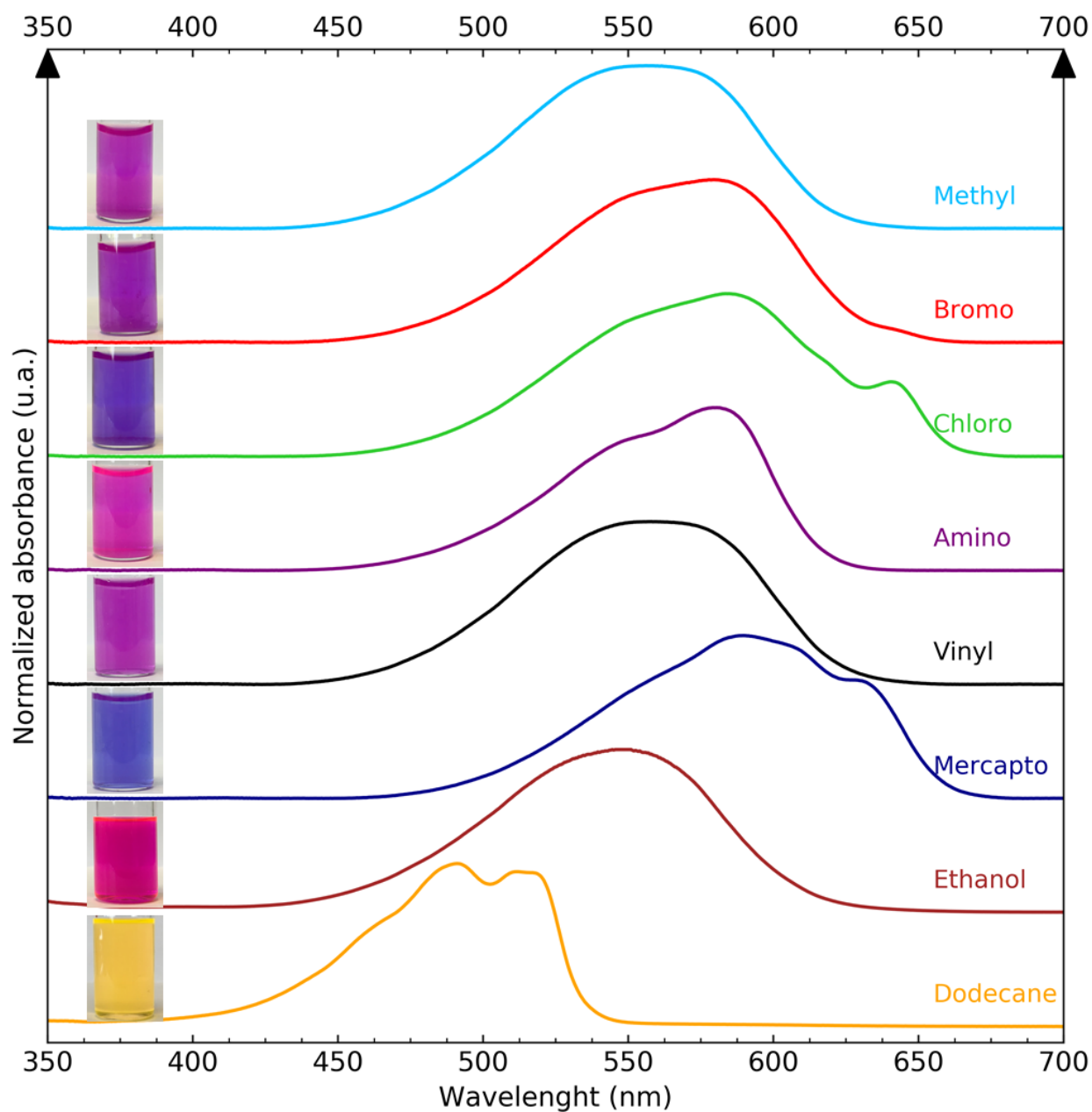


Figure 3 - Normalized absorbance of NR extracted from dodecane by methyl-Imo (cyan) and doped nanotubes: bromo (red), chloro (green), amino (purple), vinyl (black) and mercapto (dark blue). Normalized absorbance of NR in ethanol (brown) and in dodecane (orange). Optical images of the dispersions are added above their corresponding curve.

167 [References.](#)

- 168 Amara, M. S.; Paineau, E.; Rouziere, S.; Guiose, B.; Krapf, M. E. M.; Tache, O.; Launois, P.; Thill,
169 A., Hybrid, Tunable-Diameter, Metal Oxide Nanotubes for Trapping of Organic Molecules.
170 *Chemistry of Materials* **2015**,27 (5), 1488-1494.
- 171 Arancibia-Miranda, N.; Escudey, M., Imogolite-Like Family. In *Nanosized Tubular Clay Minerals:
172 Halloysite and Imogolite*, Bergaya, F., Ed. Elsevier: 2016; Vol. 7, pp 458-483.
- 173 Bahadori, E.; Vaiano, V.; Esposito, S.; Armandi, M.; Sannino, D.; Bonelli, B., Photo-activated
174 degradation of tartrazine by H₂O₂ as catalyzed by both bare and Fe-doped methyl-imogolite
175 nanotubes. *Catalysis Today* **2018**,304, 199-207.
- 176 Bottero, I.; Bonelli, B.; Ashbrook, S. E.; Wright, P. A.; Zhou, W.; Tagliabue, M.; Armandi, M.;
177 Garrone, E., Synthesis and characterization of hybrid organic/inorganic nanotubes of the imogolite
178 type and their behaviour towards methane adsorption. *Physical Chemistry Chemical Physics*
179 **2011**,13 (2), 744-750.
- 180 Boyer, M.; Paineau, E.; Bacia-Verloop, M.; Thill, A., Aqueous dispersion state of amphiphilic hybrid
181 aluminosilicate nanotubes. *Applied Clay Science* **2014**,96, 45-49.
- 182 Cradwick, P. D.; Wada, K.; Russell, J. D.; Yoshinaga, N.; Masson, C. R.; Farmer, V. C., Imogolite,
183 a hydrated aluminum silicate of tubular structure. *Nature-Physical Science* **1972**,240 (104), 187-
184 189.
- 185 Dias, L. C.; Custodio, R.; Pessine, F. B. T., Theoretical studies of Nile Red by ab initio and
186 semiempirical methods. *Chemical Physics Letters* **1999**,302 (5-6), 505-510.
- 187 Dutta, A. K.; Kamada, K.; Ohta, K., Spectroscopic studies of nile red in organic solvents and
188 polymers. *Journal of Photochemistry and Photobiology a-Chemistry* **1996**,93 (1), 57-64.
- 189 Elliott, J. D.; Poli, E.; Scivetti, I.; Ratcliff, L. E.; Andrinopoulos, L.; Dziedzic, J.; Hine, N. D. M.;
190 Mostofi, A. A.; Skylaris, C.-K.; Haynes, P. D.; Teobaldi, G., Chemically Selective Alternatives to
191 Photoferroelectrics for Polarization-Enhanced Photocatalysis: The Untapped Potential of Hybrid
192 Inorganic Nanotubes. *Advanced Science* **2017**,4 (2), 1600153.
- 193 Hazra, P.; Chakrabarty, D.; Chakraborty, A.; Sarkar, N., Intramolecular charge transfer and solvation
194 dynamics of Nile Red in the nanocavity of cyclodextrins. *Chemical Physics Letters* **2004**,388 (1-
195 3), 150-157.
- 196 Hess, C. M.; Riley, E. A.; Palos-Chavez, J.; Reid, P. J., Measuring the Spatial Distribution of
197 Dielectric Constants in Polymers through Quasi-Single Molecule Microscopy. *Journal of Physical
198 Chemistry B* **2013**,117 (23), 7106-7112.
- 199 Jose, J.; Burgess, K., Benzophenoxazine-based fluorescent dyes for labeling biomolecules.
200 *Tetrahedron* **2006**,62 (48), 11021-11037.

201 Larkin, P. J., *IR and Raman Spectroscopy: Principles and Spectral Interpretation*. 1st edition ed.;
 202 Elsevier: 2011; p 230.

203 Lee, S. U.; Choi, Y. C.; Youm, S. G.; Sohn, D., Origin of the Strain Energy Minimum in Imogolite
 204 Nanotubes. *Journal of Physical Chemistry C* **2011**, *115* (13), 5226-5231.

205 Liao, Y.; Picot, P.; Brubach, J.-B.; Roy, P.; Le Caër, S.; Thill, A., Self-supporting thin films of
 206 imogolite and imogolite-like nanotubes for infrared spectroscopy. *Applied Clay Science* **2017**.

207 Lindern, P., Scattering experiments: Experimental aspects, initial data reduction and absolute
 208 calibration. In *Neutrons, X-rays and Light: Scattering Methods Applied to Soft Condensed Matter*,
 209 1st edition ed.; Lindner, P.; Zemb, T., Eds. Elsevier Science B.V.: Amsterdam, 2002; pp 23-48.

210 Martin, C.; Cohen, B.; Navarro, M. T.; Corma, A.; Douhal, A., Unraveling the ultrafast behavior of
 211 Nile red interacting with aluminum and titanium co-doped MCM41 materials. *Physical Chemistry*
 212 *Chemical Physics* **2016**, *18* (3), 2152-2163.

213 McBride, M.; Farmer, V.C.; Russel, J.D.; Tait, J.M.; Goodman, B.A., Iron substitution in
 214 aluminosilicate sols synthesized at low pH. *Clay Minerals* **1984**, *19*(1), 1-8

215 Picot, P.; Tache, O.; Malloggi, F.; Coradin, T.; Thill, A., Behaviour of hybrid inside/out Janus
 216 nanotubes at an oil/water interface. A route to self-assembled nanofluidics? *Faraday Discussions*
 217 **2016**, *191*, 391-406.

218 Picot, P.; Liao, Y.; Barruet, E.; Gobeaux, F.; Coradin, T.; Thill, A., Exploring hybrid imogolite
 219 nanotubes formation via Si/Al stoichiometry control. *Langmuir* **2018**, *34*(44), 13225-13234

220 Shafia, E.; Esposito, S.; Manzoli, M.; Chiesa, M.; Tiberto, P.; Barrera, G.; Menard, G.; Allia, P.;
 221 Freyria, F.S.; Garrone, E.; Bonelli, B., Al/Fe isomorphic substitution versus Fe₂O₃ clusters
 222 formation in Fe-doped aluminosilicate nanotubes (imogolite). *J. of Nanopart. Res.* **2015**, *17*(8), 336

223 Silverstein, R. M.; Webster, F. X.; Kiemle, D. J., Infrared Spectroscopy. In *Spectrometric*
 224 *Identification of Organic Compounds*, 7th edition ed.; Brennan, D.; Yee, J.; Wolfman-Robichaud,
 225 S.; Sandra, R., Eds. John Wiley & Sons: 2005; pp 72-126.

226 Singappuli-Arachchige, D.; Manzano, J. S.; Sherman, L. M.; Slowing, I. I., Polarity Control at
 227 Interfaces: Quantifying Pseudo-solvent Effects in Nano-confined Systems. *Chemphyschem*
 228 **2016**, *17* (19), 2982-2986.

229 Yoshinaga, N.; Aomine, S., Imogolite In Some Ando Soils. *Soil Science and Plant Nutrition* **1962**, *8*
 230 (3), 22-29.

231 Zanzottera, C.; Vicente, A.; Celasco, E.; Fernandez, C.; Garrone, E.; Bonelli, B., Physico-Chemical
 232 Properties of Imogolite Nanotubes Functionalized on Both External and Internal Surfaces. *Journal*
 233 *of Physical Chemistry C* **2012**, *116* (13), 7499-7506.